Electronic Supplemental Information

Tuning the electronic properties of monolayer and bilayer transition metal dichalcogenide compounds under direct out-of-plane compression

Ángel Morales García [a,b]*, Elena del Corro [c,d]*, Martin Kalbac [c], Otakar Frank [c]

[a] *Department of Physical and Macromolecular Chemistry, Faculty of Science, Charles University in Prague, Hlavova 2030, 128 43 Prague 2, Czech Republic*

[b] *Departament de Ciència de Materials i Química Física & Institut de Química Teòrica i Computacional (IQTUB), Universitat de Barcelona, c/ Martí i Franqués 1, 08028 Barcelona, Spain.*

[c] *J. Heyrovsky Institute of Physical Chemistry of the CAS, v.v.i, Dolejskova 2155/3, 182 23 Prague 8, Czech Republic.*

[d] *Catalan Institute of Nanoscience and Nanotechnology (ICN2), Campus UAB, Bellaterra, 08193 Barcelona, Spain.*

*e-mail: angel.morales@ub.edu , elena.delcorro@icn2.net

Contents

1. Modulation of out-of-plane compression

As it is described in the main text certain constraints are required to achieve successfully the out-of-plane compression regime to mimic the experimental conditions when anvil cell devices are used. These constraints are related to the atomic internal coordinates and the lattice parameters. Hence to shed light on the effect of varying the lattice parameters on the semiconductor-semimetal (SC-SM) pressure, several calculations have been carried out (Tables S1, S2 and Figure S1).

As concluded in the main text, the *X-M-X* angle in monolayer and the layer distances in bilayer TMDs are the most significant structural parameters to promote the electronic transition from semiconducting the semimetal state. Therefore, the modulation of P_{SC-SM} as a function of *a* lattice parameter is studied keeping fixed the *X-M-X* angle and the layer distances (Table S1). Although the metallization pressure changes by varying the lattice *a* parameter, there are no qualitative

differences in the transition sequence for the same $\partial a/a$. These sequences follow the same order as the ones reported in the main text, i.e. $MoS_2 > MoS_2 > WSe_2 > WS_2$ and $MoS_2 > WS_2 > MoSe_2 > WSe_2$ for mono- and bilayer TMDs compounds, respectively, moving from low to high pressure. It must be noted that the variation of P_{SC-SM} as a function of a parameter is higher for monolayer than bilayer compounds and it is reflected in the fitting analysis (Table S2). The values of slope (A) show that monolayer compounds present higher sensitivity to a parameter compared to bilayer family (Figure S1).

Table S1. Evolution of SM-SC transition pressure as a function of a parameter. Bold numbers correspond to the lattice parameter at the equilibrium position. The chalcogenides distances in bilayer structures correspond to distance between the highest and lowest chalcogenides.

MoS_2	Monolayer		Bilayer		$MoSe_2$	Monolayer		Bilayer	
a (Å)	S-Mo-S (deg)	P_{SC-SM} (GPa)	d(S-S) (Å)	P_{SC-SM} (GPa)	a (Å)	Se-Mo-Se (deg)	P_{SC-SM} (GPa)	d(Se-Se) (Å)	P_{SC-SM} (GPa)
3.17	72.657	3.06	8.2744	2.17	3.305	72.643	2.89	8.6920	2.94
3.175	72.652	2.98	8.2741	2.13	3.31	72.647	2.81	8.6922	2.89
3.18	72.655	2.89	8.2743	2.1	**3.314**	**72.613**	**2.76**	**8.6928**	**2.85**
3.183	**72.651**	**2.82**	**8.2747**	**2.07**	3.32	72.618	2.68	8.6929	2.80
3.19	72.655	2.72	8.2746	2.03	3.325	72.613	2.61	8.6927	2.76
3.195	72.620	2.65	8.2748	1.99	3.33	72.616	2.55	8.6918	2.68
3.2	72.640	2.60	8.2745	1.96	-	-	-	-	-
WS_2	Monolayer		Bilayer		WSe_2	Monolayer		Bilayer	
a (Å)	S-W-S (deg)	P_{SC-SM} (GPa)	d(S-S) (Å)	P_{SC-SM} (GPa)	a (Å)	Se-W-Se (deg)	P_{SC-SM} (GPa)	d(Se-Se) (Å)	P_{SC-SM} (GPa)
3.17	72.861	3.39	8.0104	2.48	3.30	72.904	3.14	8.5922	3.72
3.175	72.891	3.28	8.0104	2.44	3.305	72.906	3.06	8.5923	3.66
3.182	**72.820**	**3.15**	**8.0114**	**2.38**	3.31	72.909	2.99	8.5916	3.61
3.185	72.834	3.12	8.0117	2.36	**3.315**	**72.912**	**2.91**	**8.5922**	**3.55**
3.19	72.863	3.04	8.0118	2.33	3.32	72.914	2.83	8.5928	3.49
3.195	72.835	2.94	8.0118	2.29	3.325	72.916	2.76	8.5924	3.42
3.2	72.865	2.84	8.0119	2.26	3.33	72.919	2.68	8.5921	3.39

Table S2. Linear fitting parameters of P_{SC-SM} (GPa) $= A\, a(Å) + B$, where A and B are the slope and the intercept, respectively (see Figure S1).

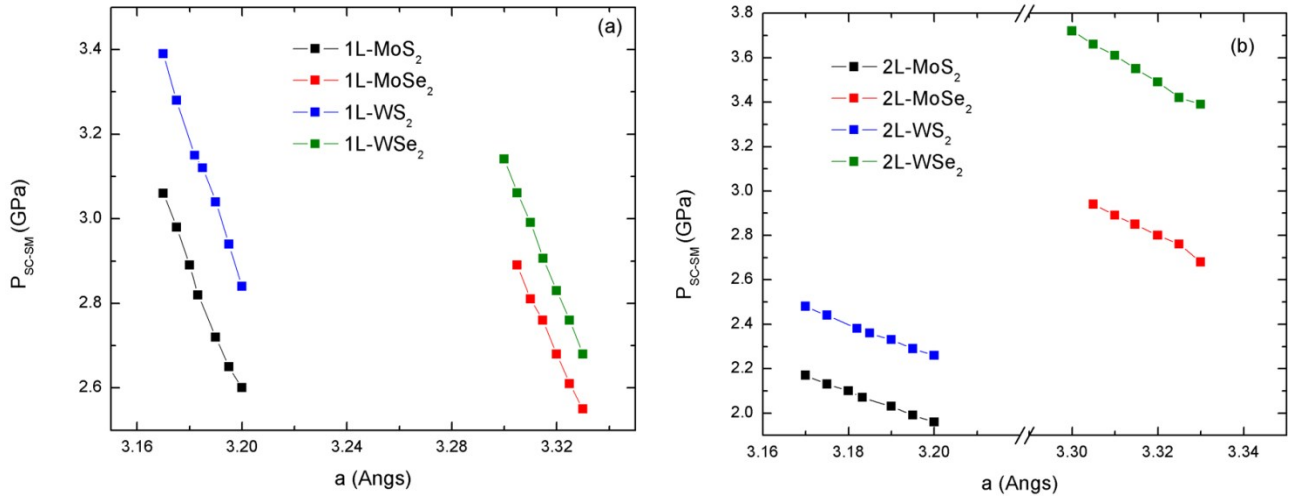| Monolayer	A (GPa/Å)	B (GPa)	Bilayer	A (GPa/Å)	B (GPa)
MoS_2	-15.73	52.92	MoS_2	-6.99	24.32
$MoSe_2$	-13.58	47.77	$MoSe_2$	-9.93	35.75
WS_2	-17.73	59.58	WS_2	-7.34	25.74
WSe_2	-15.33	53.72	WSe_2	-11.36	41.19

Figure S1. Evolution of the SC-SM pressure as a function of a parameter for (a) monolayer and (b) bilayer systems. The lines correspond to linear fitting, the slope (A) and the intercept (B) are compiled in Table S2.

2. Spin orbit coupling (SOC)

The spin-orbit coupling, which induces the splitting of the bands in K point of the Brillouin zone for both mono- and bilayer TMDs compounds, is also investigated. The most significant splitting is observed in the VB (see Figs. S2 and S3). Notice that the SOC splitting of the valence band is larger for WX_2 than for MoX_2 compounds (see Table S3). Our results are in nice agreement with the previous theoretical and experimental studies.[1-4] This spin-orbit interaction attributed to metal d orbitals further leads to strong coupling spin and valley degrees of freedom, which makes possible selective photoexcitation of carriers with various combination of valley and spin indices.
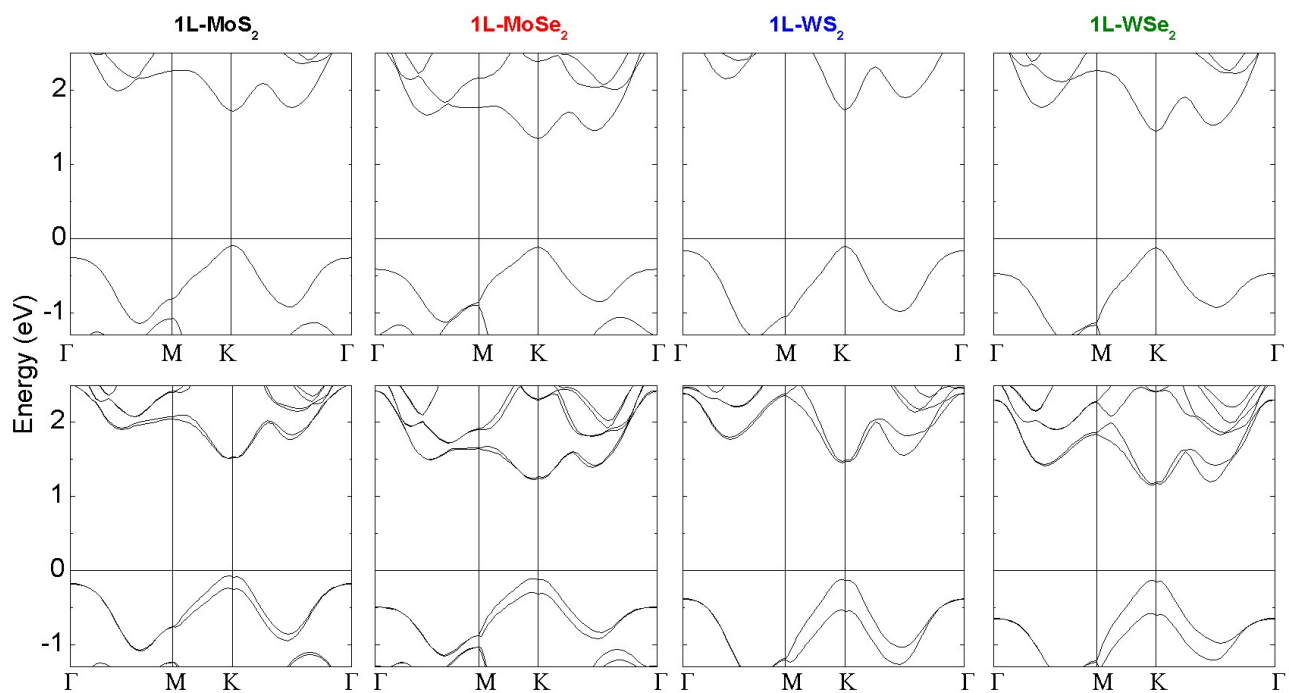
Figure S2. 1L-*MX*$_2$ band structure with (bottom panels) and without SOC (top panels).
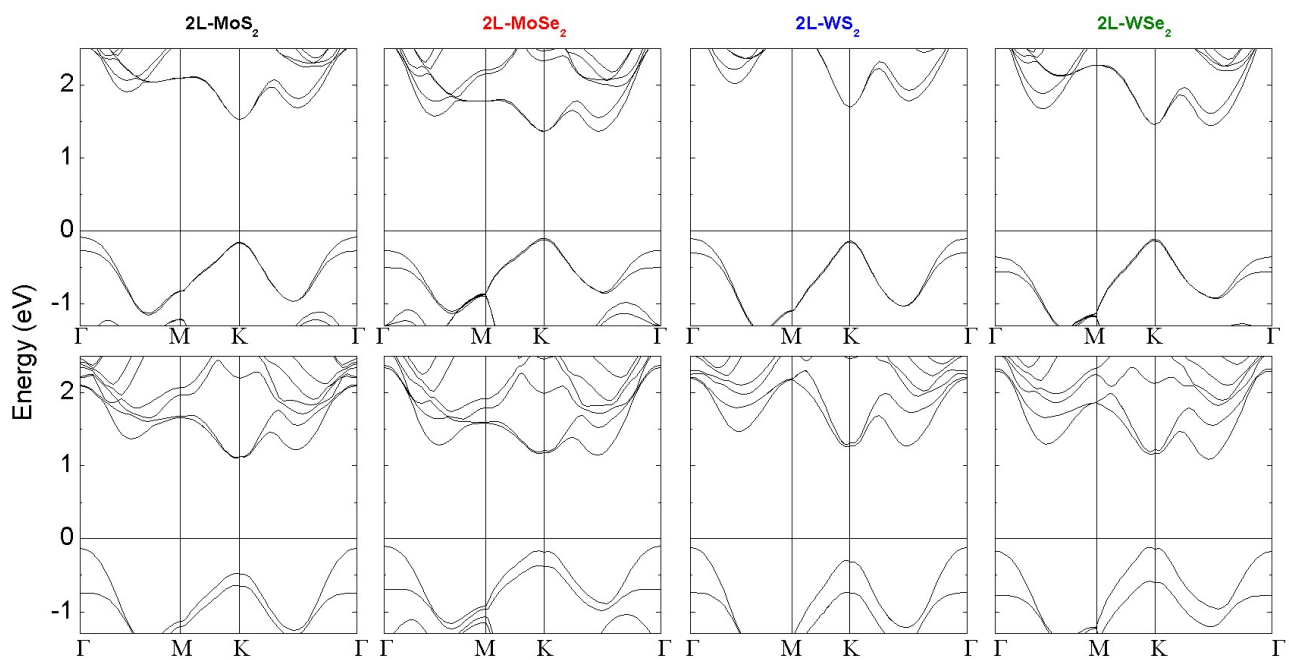

Figure S3. 2L-*MX*$_2$ band structure with (bottom panels) and without SOC (top panels).

4

Table S3. Splitting at the valence band at K for 1L- and 2L-MX_2 along with available experimental and other theoretical data. All the energies are in eV.

	MoS$_2$	WS$_2$	MoSe$_2$	WSe$_2$
	Monolayer			
our work	0.159	0.405	0.188	0.448
other GGA	0.146 [1]	0.425 [1]	0.183 [1]	0.461 [1]
experimental	0.150 [2]	-	0.180 [1]	-
	Bilayer			
our work	0.160	0.433	0.203	0.463
other GGA	0.170 [3]	-	-	0.430 [4]
experimental	0.170 [1]	-	-	-

3. Effect of the exchange-correlation functional on the band gap energy

The single layered MoS$_2$ is selected to investigate the effect of the exchange-correlation functional on the band gap energy (Table S4). PBE functional with and without SOC+D3 effects is selected along with top of hybrid (PBE0 and a modified version with 12.5% of Fock exchange) functionals. The hybrid functionals clearly overestimate the band gap whereas the PBE functional with and without SOC+D3 underestimates it. In conclusion, a standard PBE calculation reports the most accurate band gap.

Table S4. Analysis of the band gap property of 1L-MoS$_2$ using different exchange-correlation functionals.

	Band gap
PBE	1.82
PBE+SOC+D3	1.57
PBEx	2.45
PBE0	2.82
Exp [5]	1.85

4. Structural and Electronic relationship at PBE level

Figure S4 is analogous to Figure 3 including its interpretation. The data shown in Figure S4 correspond to PBE level. 1L-MoX_2 compounds undergo to metal state at lower stress than 1L-WX_2 compounds. On the other hand, 2L-MS$_2$ compounds metallize before 2L-MSe$_2$ compounds.
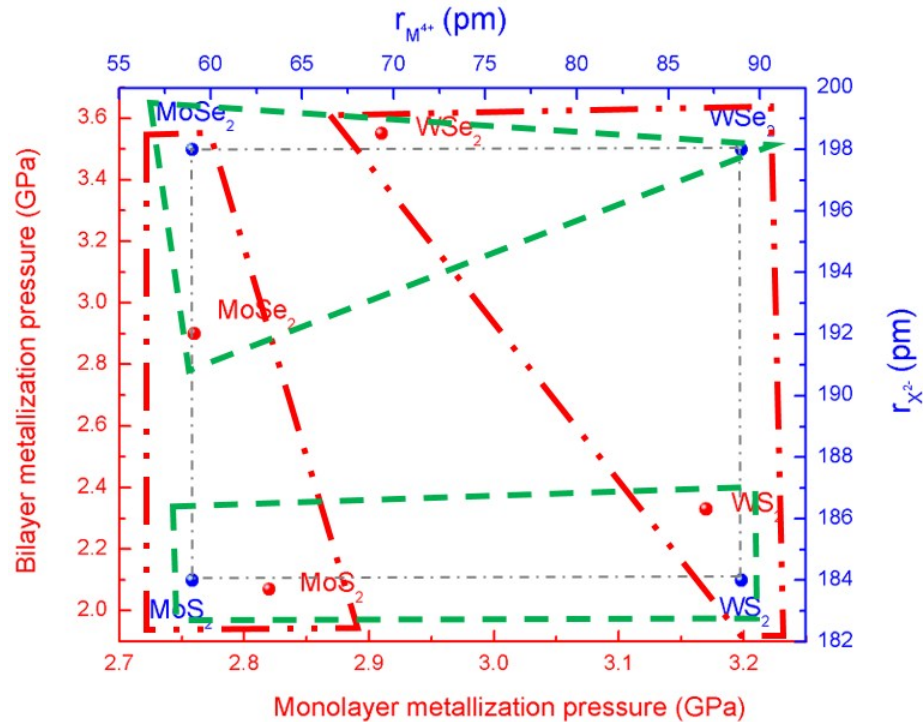

Figure S4. Blue, and red axes correspond to atomic radii and direct-to-indirect, semiconductor-to-semimetal transition stresses, respectively. Blue spots correspond to the location of MX_2 compounds as a function of M^{4+} and X^{2-} radius and gray spots reflect the relation between the two electronic transitions. Red dash-pointed lines indicate the semiconductor-semimetal transition, where the MoX_2 compound require the lowest strain. Green dashed lines correspond to direct-to-indirect transition where the MS$_2$ compounds show the lowest strain.

[1] A. Ramasubramaniam, *Phys. Rev. B*, 2012, **86**, 115409.

[2] K. F. Mak, C. Lee, J. Hone, J. Shan and T. F. Heinz, *Phys. Rev. Lett.*, 2010, **105**, 136805.

[3] A. Ramasubramaniam, D. Naveh and E. Towe, *Phys. Rev. B*, 2011, **84**, 205325.

[4] H. Zeng, G.-B. Liu, J. Dai, Y. Yan, B. Zhu, R. He, L. XIe, S. Xu, X. Chen, W. Yao and X. Cui, *Sci. Rep.* 2013, **3**, 1608.

[5] M. Peña-Alvarez, E. del Corro, A. Morales-García, L. Kavan, M. Kalbac and O. Frank, *Nano Lett.*, 2015, **15**, 3139-3146.